

A somitic Wnt16/Notch pathway specifies haematopoietic stem cells

Wilson K. Clements¹, Albert D. Kim¹, Karen G. Ong¹, John C. Moore², Nathan D. Lawson² & David Traver¹

Haematopoietic stem cells (HSCs) are a self-renewing population of cells that continuously replenish all blood and immune cells during the lifetime of an individual^{1,2}. HSCs are used clinically to treat a wide array of diseases, including acute leukaemias and congenital blood disorders, but obtaining suitable numbers of cells and finding immune-compatible donors remain serious problems. These difficulties have led to an interest in the conversion of embryonic stem cells or induced pluripotent stem cells into HSCs, which is not possible using current methodologies. To accomplish this goal, it is critical to understand the native mechanisms involved in the specification of HSCs during embryonic development. Here we demonstrate in zebrafish that Wnt16 controls a novel genetic regulatory network required for HSC specification. Non-canonical signalling by Wnt16 is required for somitic expression of the Notch ligands *deltaC* (*dlc*) and *deltaD* (*dld*), and these ligands are, in turn, required for the establishment of definitive haematopoiesis. Notch signalling downstream of Dlc and Dld is earlier than, and distinct from, known cell-autonomous requirements for Notch, strongly suggesting that novel Notch-dependent relay signal(s) induce the first HSCs in parallel to other established pathways. Our results demonstrate that somite-specific gene expression is required for the production of haemogenic endothelium.

We wished to define better the role, if any, of Wnt signalling in HSC specification during embryonic development. Although Wnt signalling can exert strong effects on adult HSCs, an *in vivo* regulatory function is controversial, and the role of Wnt signalling in establishing haematopoiesis during development is unclear². Wnt signalling pathways have been loosely grouped into two families: canonical and non-canonical^{2,3}. Canonical signalling is defined by stabilization of β -catenin, which in cooperation with lymphoid-enhancer-binding factor/T-cell factor (*Lef/Tcf*) DNA-binding proteins, activates transcription of Wnt target genes^{2,3}. Non-canonical signalling is β -catenin/Tcf-independent, with less well-characterized intracellular pathways³. Disruption of canonical signalling in zebrafish by targeted deletion of *wnt3a* results in HSC deficits², but these animals have massive morphological defects, including near absence of the caudal tissues⁴ where HSCs arise during embryogenesis. Canonical Wnt signalling by unknown ligands also seems to have a role in maintaining and/or expanding very early HSCs in cooperation with prostaglandins⁵. At present, no studies have demonstrated an absolute requirement for Wnt signalling in the earliest specification of recognizable HSCs, and no requirement for β -catenin/Tcf-independent, non-canonical signalling has been reported.

We searched for candidate Wnt proteins expressed near pre-haematopoietic mesoderm and identified a previously uncharacterized zebrafish *wnt16* orthologue (Supplementary Fig. 1) expressed in the dorso-anterior portion of more rostral somites from 10 h post fertilization (h.p.f.; tailbud stage) to 24 h.p.f. (Supplementary Fig. 2), the time frame when pre-haematopoietic mesoderm transitions to recognizable HSC precursors in the dorsal aorta. *Wnt16* is conserved across vertebrate phyla (Supplementary Fig. 1), and the human form was originally identified as a gene inappropriately expressed in pre-B-acute lymphoblastic

leukaemia (ALL) cells containing the E2A-PBX1 t(1;19) translocation product⁶. In zebrafish, two *wnt16* splice variants are produced, only one of which is active (Supplementary Figs 1a, b and 3 and Supplementary Table 1).

Knock down of Wnt16 by injection of either of two 'splice-blocking' morpholinos (W16MO) caused a striking haematopoietic phenotype. Morpholinos alone or in combination reduced levels of functional *wnt16* mRNA (Supplementary Figs 1a and 4), yielding highly similar phenotypes in comparison to a 5-base-pair mismatch control morpholino, which had no effect (Supplementary Figs 4 and 5). Whole-mount *in situ* hybridization (WISH) revealed that HSC precursors, a population of *runx1*⁺ cells in the ventral floor of the dorsal aorta^{1,7,8}, as in mouse⁹, are absent in embryos injected with W16MO at 24 h.p.f. (red arrowhead; Fig. 1a, b and Supplementary Table 2). By 33 h.p.f., HSCs can be observed as a population of *cmyb*⁺ cells between the dorsal aorta and posterior cardinal vein¹, and this population is also absent in W16MO-injected embryos (red arrowhead, Fig. 1c, d and Supplementary Table 2). HSCs observable in living transgenic animals carrying *GFP* under the control of the *cd41* (also known as *itga2b*) promoter^{10–12} are absent or reduced in *wnt16* morphants (red arrowheads, Fig. 1e, f; see also Supplementary Movies 1 and 2 and Supplementary Table 2), as are unique double-positive cells in *kdr1:RFP* and *cmyb:GFP* double transgenics⁷ (Fig. 1g, h, yellow cells; see also Supplementary Table 2), whereas unrelated GFP-labelled multiciliate cells in the pronephros are unaffected (yellow arrowheads in Fig. 1e, f and green cells in Fig. 1g, h). Generation of T lymphocytes requires an HSC precursor^{10,11,13}, providing a useful readout for whether HSCs have been specified or not. In *cd41:GFP* transgenic animals, GFP⁺ HSCs retain residual fluorescence as they differentiate into the first thymic lymphocytes around 3 days post fertilization (d.p.f.)¹⁰, and these thymic immigrants are greatly reduced in *wnt16* morphants (Supplementary Movies 3 and 4). Accordingly, *wnt16* morphants lack *rag1*⁺ T lymphocytes at 4.5 d.p.f. (blue arrows, Fig. 1i, j and Supplementary Table 2), despite intact thymic epithelium (Supplementary Fig. 6). Together, our results indicate that Wnt16 is required for the specification of HSCs during embryonic development.

To determine the specificity of W16MO-induced defects, we examined the integrity of non-haematopoietic tissues by morphology and expression of marker genes (Fig. 2 and Supplementary Table 3). *Wnt16* morphants are grossly normal (Fig. 2a, b), with intact and functional vasculature, as evidenced by beating hearts and circulating primitive, non-HSC-derived erythroid cells, although there appear to be subtle patterning defects in the number and position of intersegmental vessels. WISH revealed that W16MO-injected embryos have primitive blood (*gata1*; Fig. 2c, d and Supplementary Table 3), somites (*myod*; Fig. 2e, f and Supplementary Table 3), vasculature (*tll1*, *cdh5* and *kdr1* (also called *flk1*); Fig. 2g–l and Supplementary Table 3), dorsal aorta (*efnb2a*; Fig. 2m, n; *notch1b*, *notch3*, *dll4*; Supplementary Fig. 7a–d, o, p and Supplementary Tables 3 and 5), hypochord (*col2a1a*; Fig. 2o, p and Supplementary Table 3), notochord and floorplate (*shha*; Fig. 2q, r and Supplementary Table 3), and pronephros (*cdh17*; Fig. 2s, t and

¹Department of Cellular and Molecular Medicine and Section of Cell and Developmental Biology, University of California at San Diego, 9500 Gilman Drive, La Jolla, California 92093-0380, USA. ²Program in Gene Function and Expression, University of Massachusetts Medical School, Worcester, Massachusetts 01605, USA.

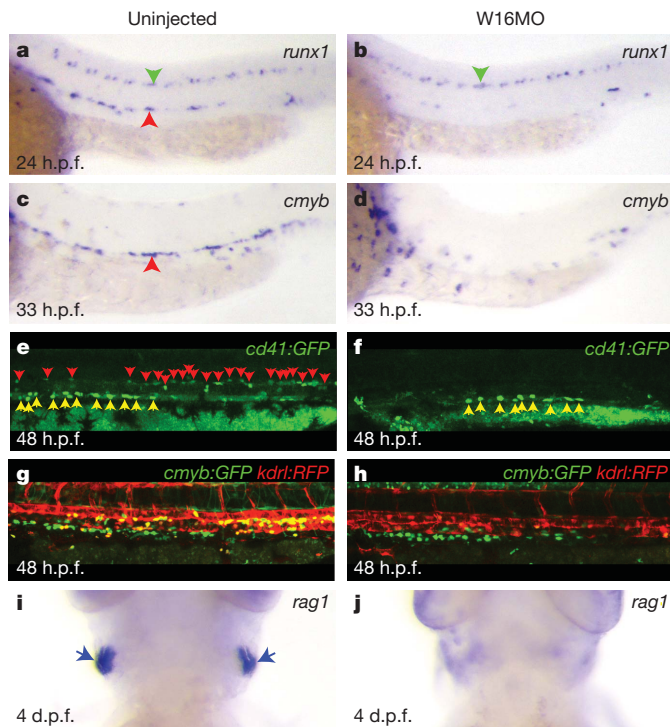


Figure 1 | *Wnt16* is required for the specification of HSCs. **a–d**, Expression of the HSC markers *runx1* (**a, b**) and *cmyb* (**c, d**). **e–h**, Fluorescently labelled HSCs in *cd41:gfp* (**e, f**) and *cmyb:GFP;kdr1:RFP* transgenics (**g, h**). **i, j**, Expression of the lymphocyte marker *rag1*. Embryos are either uninjected (left column) or injected with 5 ng W16MO (right column). Red arrowheads identify the aorta region (**a, c**) or individual HSCs (**e**). Green arrowheads identify unaffected *runx1*⁺ neurons (**a, b**). Yellow arrowheads identify unaffected GFP⁺ multiciliate cells of the pronephros (**e, f**). Yellow cells are HSCs (**g**). Blue arrows identify thymic T cells (**i**). **a–h**, Dorsal up, anterior left. **i–j**, Ventral views, anterior up. Original magnification at $\times 200$.

Supplementary Table 3). Thus, defects in HSC specification in *wnt16* morphant animals are highly specific and not due to wholesale failure in the specification of nearby tissues.

Canonical, β -catenin/Tcf-dependent Wnt signalling has been reported to be involved in HSC specification in mice² and very early maintenance in zebrafish⁵. We therefore wanted to determine if Wnt16 is canonical. Overexpression of Wnt16 caused phenotypic defects, demonstrating active protein (Supplementary Fig. 3), but in comparison to Wnt3 (ref. 14) it did not cause ectopic expression of canonical targets (Supplementary Fig. 8). Conversely, Wnt16 knock down caused no decrease in canonical reporter activity (Supplementary Fig. 9). Thus, Wnt16 does not act via β -catenin/Tcf and must act via a non-canonical pathway, as has been suggested for human WNT16B (refs 15, 16). Loss of other non-canonical Wnt ligands causes distinct phenotypes. Loss of Wnt5b is much more severe, causing nearly complete absence of primary trunk vasculature¹⁷, whereas loss of Wnt11 had no effect on HSC specification (Supplementary Fig. 10 and Supplementary Table 4). We therefore conclude that the HSC defects caused by loss of *wnt16* are not a general consequence of loss of non-canonical Wnt signalling.

Notch signalling is required across phyla for the developmental specification of HSCs¹. Global inhibition of Notch signalling by mutation or targeted deletion of *mind bomb* (*mib*)—which is required for Notch ligand activity—or the essential Notch DNA-binding co-factor *Rbpjk* results in total loss of HSCs, as well as severe vascular defects¹. If Wnt16 were to regulate Notch pathway genes, this regulation might explain the loss of HSCs in *wnt16* morphant animals. The specific ligands and receptors required in zebrafish for specification of HSCs by the Notch pathway have not been determined. We therefore examined

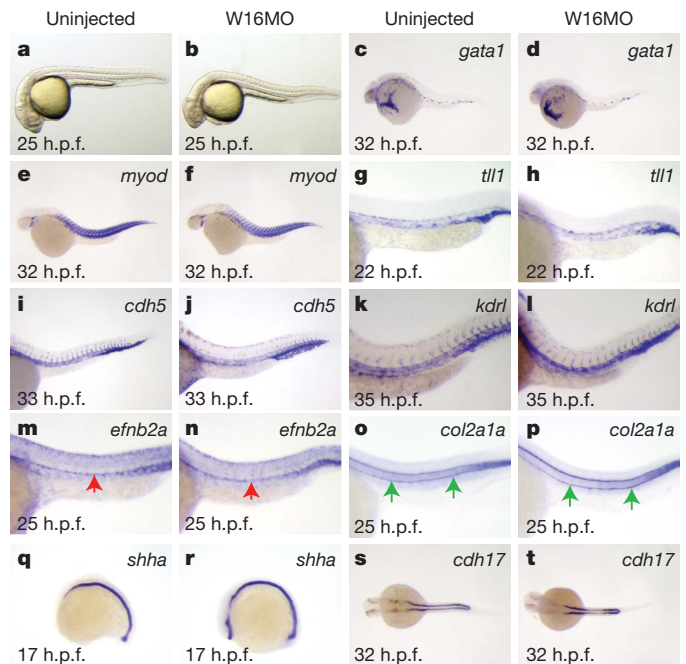


Figure 2 | The *wnt16* loss-of-function phenotype is specific. **a–t**, Uninjected or W16MO-injected embryos in bright-field (**a, b**) or processed by WISH for tissue-specific genes: primitive blood (*gata1*, **c, d**), somites (*myod*, **e, f**), vasculature (*tll1*, **g, h**; *cdh5*, **i, j**; *kdr1*, **k, l**), dorsal aorta (*efnb2a*, **m, n**), hypochord (*col2a1a*, **o, p**), floorplate and notochord (*shha*, **q, r**), or pronephros (*cdh17*, **s, t**) at the developmental times indicated. Red arrows, dorsal aorta (**m, n**); green arrows, hypochord (**o, p**). Anterior left. **a–r**, Dorsal up. **s, t**, Dorsal views. **a–f, q–t**, Original magnification at $\times 64$; **g–p**, original magnification at $\times 200$.

comparative expression of Notch ligands and receptors that might participate in HSC specification in uninjected or W16MO-injected animals. Most Notch receptors and ligands were either unaffected or very weakly affected (Supplementary Fig. 7 and Supplementary Table 5). However, expression of two Notch ligands, *dlc* and *dld*, was markedly decreased in somites at 17 h.p.f. (16-somite stage (ss); Fig. 3a–d and Supplementary Table 5). In accord with decreased somitic ligand expression, Notch reporter activity was decreased in somites at 17.5 h.p.f. (Supplementary Fig. 11). Interestingly, diminution of *dlc* and *dld* was tissue specific, because expression was maintained in pre-somitic mesoderm (Fig. 4a–d), and *dlc* expression in the dorsal aorta appeared relatively normal at 22 h.p.f. (Supplementary Fig. 12 and Supplementary Table 5). Although Wnt16 function is required for somitic expression of *dlc* and *dld*, we see no evidence for reciprocal regulation of *wnt16* by Dlc and Dld (Supplementary Fig. 13), or indeed by Notch at all, as expression is unaffected in *mib* mutants (not shown).

To determine whether alterations in the expression of *dlc* and/or *dld* might explain the decrease in HSCs we observe in *wnt16* morphant animals, we tested whether loss of function in these genes alone or in combination could alter HSC specification. *Beamter* (*bea*) mutants carry a predicted null allele of *dld*¹⁸. We compared HSC and T-lymphocyte marker expression in wild-type embryos, homozygous *bea* mutants, embryos injected with *dld* morpholino (*dld*MO)¹⁹, and homozygous *bea* mutants injected with *dld*MO. We found that *runx1* transcripts at 24 h.p.f., and *cmyb* at 36 h.p.f., were greatly reduced in *bea* homozygous mutants and embryos injected with *dld*MO (Fig. 3e–g, i–k and Supplementary Table 6), but an apparent recovery of HSCs had occurred by 4.5 d.p.f., when *rag1* transcripts (revealing the thymic progeny of HSCs) were readily visible in both groups (Fig. 3m–o and Supplementary Table 6). Combinatorial reduction of Dlc and Dld activity, however, eliminated HSCs, as revealed by elimination of *runx1* transcripts at 24 h.p.f. (Fig. 3h and Supplementary Table 6), *cmyb* transcripts at 36 h.p.f. (Fig. 3l and Supplementary Table 6) and

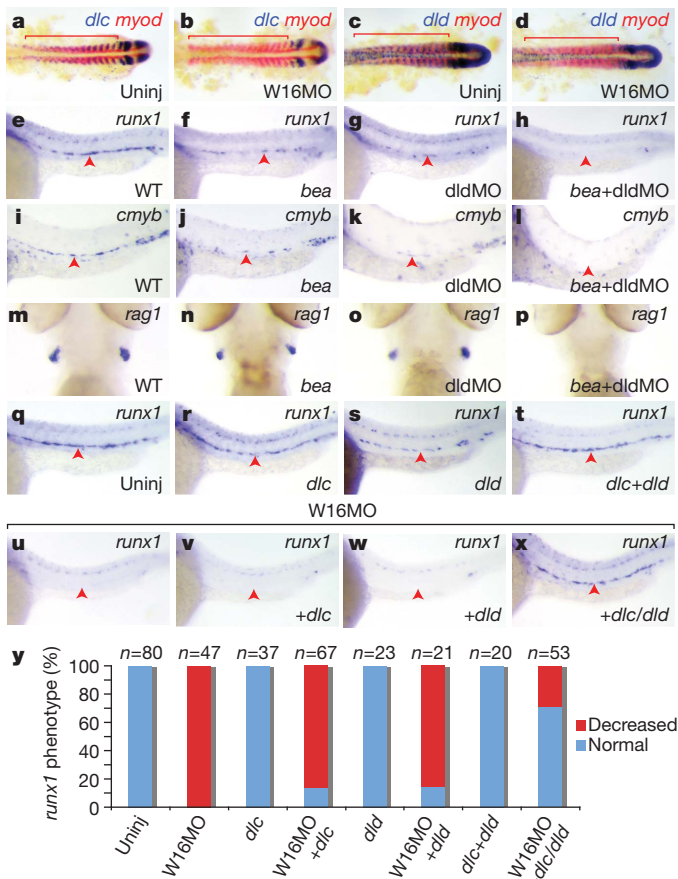


Figure 3 | Wnt16 acts upstream of Notch ligands Dlc and Dld.

a–d, Expression of somitic *dlc* (**a**, **b**) and *dld* (**c**, **d**) but not *myod* (red) is decreased at 17 h.p.f. in W16MO-injected embryos. Red bars indicate somites. **e–l**, Expression of the HSC markers *runx1* at 24 h.p.f. (**e**–**h**) and *cmyb* at 36 h.p.f. (**i**–**l**) is reduced in *dlc* mutant (*bea*) embryos (**f**, **j**) or *dld*MO-injected embryos (**g**, **k**), and eliminated in the combined animals (**h**, **l**). **m–p**, The lymphocyte marker *rag1* at 4.5 d.p.f. is present in wild-type (**m**, WT), *bea* (**n**) and *dld*MO-injected animals (**o**), but eliminated in *bea* embryos injected with *dld*MO (**p**). **q–x**, Combined injection of *dlc* and *dld* rescues HSCs in *wnt16* morphants. *Runx1* at 24 h.p.f. One group of embryos was uninjected, or injected with the indicated Notch ligand mRNAs alone (**q–t**). A second group of W16MO-injected embryos was co-injected with Notch ligand mRNAs (**u–x**). **y**, Percentages of embryos displaying the depicted phenotypes. **a–d**, $\times 100$ (original magnification) views of flat mounts, anterior left. **e–l**, $\times 200$ (original magnification) lateral views, anterior left, dorsal up. **m–p**, $\times 200$ (original magnification) ventral head views, anterior up. Red arrowheads indicate the aorta region.

rag1 transcripts at 4.5 d.p.f. (Fig. 3p and Supplementary Table 6). Thus, *dlc* and *dld* are combinatorially required for specification of HSCs in zebrafish, and their diminished expression in the somites of *wnt16* morphant animals can, in principle, explain the observed loss of HSCs.

To confirm that the loss of HSCs in *wnt16* morphants is due to loss of *dlc* and *dld*, we performed a rescue experiment. We injected embryos with W16MO, and in some cases co-injected mRNA encoding full-length Dlc and Dld ligands singly or in combination. Injection of *dlc* and *dld* mRNA alone or in combination did not have a strong effect on HSC numbers, as measured by *runx1*⁺ cells in the dorsal aorta (Fig. 3q–t, y). Co-injection of individual mRNAs with W16MO was unable to restore *runx1* transcript levels (Fig. 3u–w, y). However, when injected together, *dlc* and *dld* restored *runx1*⁺ HSCs in a high percentage of W16MO-injected animals (Fig. 3x, y). These results confirm that decreased *dlc* and *dld* expression in *wnt16* morphants is responsible for loss of HSCs.

Studies in zebrafish and mice have shown that Notch specification of HSCs is regulated by Shh and VegfA (ref. 1). Shh regulates the

expression of *vegfa*, and VegfA signalling is, in turn, required for the vascular expression of Notch receptor genes¹. Notch signalling is required for both arteriovenous and HSC specification^{1,20–24}. In accord with these observations, loss of Shh signalling causes loss of both artery and HSCs¹. Taken together, one level of control over HSC specification seems to be through a Shh/VegfA/Notch signalling pathway¹. Shh/VegfA/Notch specification of HSCs seems to be distinct from Wnt16/Dlc/Dld effects because vascular and arterial specification is unaffected in W16MO animals (Fig. 2i–n and Supplementary Fig. 7a–d, o, p). Moreover, *shha* and Notch receptor expression are unaffected in W16MO animals (Fig. 2q, r and Supplementary Fig. 7a–l). To confirm that these pathways are discrete, we examined the expression of six known Shh target genes, with particular interest in *vegfa*. None of the Shh targets examined showed significantly altered expression (Supplementary Fig. 14 and Supplementary Table 7). Our results indicate that the Wnt16 and Shh pathways act in parallel upstream of HSC specification.

The predominant model for how Notch signalling regulates HSC specification is that endothelial cells of the dorsal aorta receive a requisite Notch1-mediated signal^{1,21–24}. Chimaeric mice generated using Notch1-deleted cells show no contribution of knockout cells to the adult haematopoietic system, demonstrating that Notch1 signalling is required cell-autonomously for specification of HSCs^{1,21}. The relevant Notch ligand(s) are thought to be expressed in the formed dorsal aorta and/or immediately surrounding mesenchyme^{1,22–24}. A contributing ligand seems to be *Jag1*, because *Jag1*-knockout mice have severely impaired, but not totally abrogated, development of HSCs^{1,24}. Notch1 activation of *Runx1* is thought to occur indirectly through *Gata2*, as the *Runx1* promoter does not contain identifiable *Rbpjk* binding sites^{1,21,23,24}. Notch signalling defects in *wnt16* morphants indicate that the requirement for Dlc and Dld is not the same as this cell-autonomous requirement, because decreased Notch ligand expression is specific to somites (Fig. 3a–d), whereas expression of *dlc* is normal in the dorsal aorta of *wnt16* morphants (Supplementary Fig. 12 and Supplementary Table 5) and *dld* is not natively expressed near the formed dorsal aorta. Moreover, expression of *jag1b* and its putative target *gata2* are unaffected in *wnt16* knock down animals (Fig. 4a–d).

To understand better whether Dlc/Dld specification of HSCs works cell-autonomously or not, we sought to define the timing of the Notch signalling event that is absent in W16MO-injected animals using animals carrying transgenes that allow heat-shock induction of the Notch intracellular domain (NICD), which is a dominant activator of the Notch pathway^{20,25}. We induced NICD expression at different time points to identify the temporal window when enforced Notch activity could rescue HSC expression in *wnt16* morphants. Nuclear, Myc-tagged NICD protein is present in transgenic animals by 1 h post heat shock, and is strong from 3 h post heat shock (Fig. 4e–h) through to at least 24 h post heat shock (not shown), consistent with previous reports²⁶. Heat-shock induction of NICD at 14 h.p.f. (10-ss) rescued *cmyb* expression at 36 h.p.f. (Fig. 4i–k and Supplementary Table 8), as has been seen previously for rescue of *mib*²⁰. Surprisingly, heat shock just 2 h later (14-ss) did not rescue *cmyb* expression along the dorsal aorta (red circle, Fig. 4l and Supplementary Table 8). These results indicate that the critical phase of Notch signalling required for HSC specification downstream of Wnt16 occurs between 15–17 h.p.f. (12–16-ss) and abruptly terminates by about 18–19 h.p.f. (18–20-ss).

Because this timing is well before the formation of the dorsal aorta and HSCs from its ventral endothelium, we sought to determine when cells fated to become HSCs first experience a cell-autonomous Notch signal. First, we used a *tp1:Kaede* Notch reporter line expressing a green-to-red, photoconvertible Kaede protein under the control of a Notch-responsive promoter. Photoconversion of Notch-responsive, Kaede⁺ cells in the Dlc/Dld-critical window, before 19.5 h.p.f. (21-ss), yielded converted, red fluorescent progeny that contributed to the region near the dorsal aorta at 3 d.p.f. (left panels of Fig. 4m, n), but these cells never became HSCs, as shown by their failure to produce

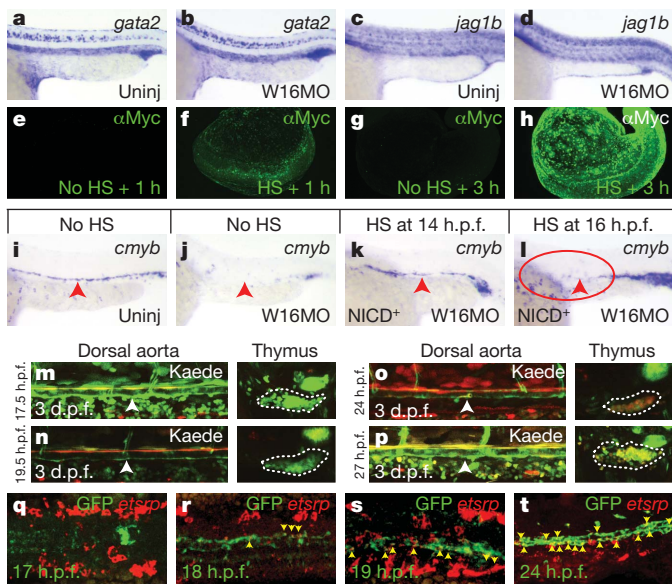


Figure 4 | Non-cell-autonomous requirement for Notch in HSC specification. **a–d**, Expression of the Notch target *gata2* (**a, b**) and the Notch ligand *jag1b* (**c, d**) in uninjected (**a, c**) or W16MO-injected (**b, d**) embryos at 22 h.p.f. **e–h**, Whole-mount immunofluorescence visualization of the Myc-tagged NICD at 1 h (**e, f**) and 3 h (**g, h**) after either no induction (**e, g**) or heat-shock (HS) induction (**f, h**). **i–l**, *Cmyb* expression at 36 h.p.f. in transgenic animals carrying a heat-shock-inducible dominant activator of Notch signalling (NICD) in uninjected (**i**), W16MO-injected (**j**), W16MO-injected and heat-shock induced at 14 h.p.f. (10-ss; **k**) or 16 h.p.f. (14-ss; **l**). Red arrowheads indicate the dorsal aorta region. Red circle indicates the area where HSCs should normally be expressed (**l**). **m–p**, Green-to-red photoconvertible Kaede Notch reporter animals were entirely photoconverted at the times indicated at the left of each panel pair and imaged at 3 d.p.f. Confocal images of the dorsal aorta (white arrowheads; left panels of **m–p**) and thymus (dashed white outline; right panels of **m–p**) reveal photoconverted cells only in the thymi of fish converted at 24 and 27 h.p.f. (right panels of **o, p**). **q–t**, Max-projection confocal images of the trunk region of embryos processed by double fluorescence *in situ* for a Notch transgene *GFP* (green) and the haematopoietic mesoderm marker *etsrp* (red) at the times indicated. Yellow arrowheads indicate double-positive cells (**r–t**). **a–d, i–l**, $\times 200$ (original magnification) lateral views of the trunk region, anterior left, dorsal up. **e–h**, $\times 100$ (original magnification) whole-embryo views. **m–p**, $\times 200$ (original magnification) lateral views of the dorsal aorta (left panels). **m–p**, Single thymic lobes (right panels). **q–s**, Cropped, $\times 200$ (original magnification) dorsal views, anterior left. **t**, Cropped, $\times 100$ (original magnification) lateral aorta view, anterior left, dorsal up.

labelled thymic progeny (right panels of Fig. 4m, n). In contrast, photoconversion at 24 h.p.f. and later time points produced both labelled dorsal aorta (left panels of Fig. 4o, p) and thymic immigrants (right panels of Fig. 4o, p). Because there is a lag between reception of a Notch signal and the production of mature Kaede protein in the reporter lines, we wanted to confirm when Notch activity appears in pre-haematopoietic cells by a more immediate readout for Notch responsiveness. We performed double fluorescence *in situ* analysis in *tp1:GFP* Notch-reporter transgenic animals for expression of *GFP* and *etsrp*, which labels pre-haematopoietic mesoderm and is required for HSC specification²⁷. The very first double-labelled cells appeared at 18 h.p.f. in the midline (Fig. 4q, r), and increased in number through to at least 24 h.p.f. (Fig. 4s, t). Taken together, our data indicate that Notch signalling in cells fated to become HSCs begins after 18 h.p.f. and continues well into the second day of development. This timing fits well with the established model of cell-autonomous Notch specification of HSCs, where Notch signalling in nascent HSCs occurs after aortic specification via interactions between *Jag1b* and Notch1 (refs 1, 21–24). Overall, our results indicate that somitic signalling by Dlc and Dld downstream of Wnt16 is temporally and spatially distinct from the

observable cell-autonomous requirement for Notch signalling. Wnt16 therefore controls a previously unappreciated environmental requirement for Notch signalling in the somites, most simply explained by regulation of an unidentified relay signal.

To understand better what cell population Wnt16-regulated somitic Dlc and Dld act on, we examined fine somite patterning in Wnt16 and Dlc/Dld loss-of-function animals. Because somite segmentation (Figs 2a, b, e, f and 3a–d) and myotomal specification (Figs 2e, f and 3a–d) appear to be intact in *wnt16* morphants, we examined specification of the sclerotomal somite compartment, which houses vertebral and vascular smooth muscle cell precursors. Sclerotomal markers displayed severely decreased expression, albeit to variable extents, in both W16MO and combined *dld/dld* loss of function animals (Supplementary Fig. 15 and Supplementary Table 9). Although hypochord (Supplementary Fig. 15u–y, green arrowheads) was abolished in the *dld/dld* double loss-of-function animals (Supplementary Fig. 15x), as has been reported¹⁸, hypochord was specified normally in *wnt16* morphants (Fig. 2o, p and Supplementary Fig. 15y), emphasizing the fact that the Wnt16-dependent loss of somitic *dld/dld* is distinct from global loss. Our results indicate that sclerotome specification or morphogenesis is required for HSC specification.

Our results demonstrate that non-canonical signalling by Wnt16 is required genetically upstream of the combined actions of the Notch pathway ligands Dlc and Dld for HSC specification. Dlc/Dld-mediated Notch signalling is spatially and temporally distinct from previously described cell-autonomous requirements for Notch in HSC specification, pointing to the possibility of a novel relay signal. These data represent the first demonstration, to our knowledge, that non-canonical Wnt signalling activity is required for HSC specification in vertebrates. Given that *Wnt16* in mouse is expressed at similar times of development²⁸ and is expressed in embryoid bodies during commitment to blood and vasculature²⁹, it is feasible that this function is conserved in mammals.

METHODS SUMMARY

Zebrafish strains. The following strains were maintained in accordance with IACUC approved procedures: AB*, *Tg(TOP:GFP)^{w25}*, *Tg(-6.0itga2b:eGFP)^{la2}*, *Tg(hsp70l:Gal4)^{1.5kca4}*, *Tg(UAS:myc-Notch1a-intra)^{kca3}*, *Tg(tp1-MmHbb:EGFP)^{um14}*, *Tg(tp1-MmHbb:Kaede)^{um15}*, *Tg(cmyb:EGFP)^{z169}*, *Tg(kdr:l:RFP)^{la4}* and *dld^{it446/it446}*.

Constructs. Probes and mRNA were synthesized from published constructs or cloned *de novo* according to standard procedures.

Morpholinos. The following morpholinos were used: 5 ng W16MO1 (AGGTTAGTTCGTGACCCACCTGTC), W16MO2 (GCGTGGAACTACTACATCCA ACTTC) and W16CoMO (AcGTTAGTGTGTGAgCCAgCTcTC; lowercase letters denote mismatched bases).

Genotyping and PCR. Genotyping and PCR were performed by standard methods using primers and conditions described in Methods.

Whole-mount *in situ*, antibody staining and microscopy. These were performed according to standard methods and are described in full in Methods.

Full Methods and any associated references are available in the online version of the paper at www.nature.com/nature.

Received 6 May 2010; accepted 11 April 2011.

- Gering, M. & Patient, R. Notch signalling and haematopoietic stem cell formation during embryogenesis. *J. Cell. Physiol.* **222**, 11–16 (2010).
- Staal, F. J. & Luis, T. C. Wnt signaling in hematopoiesis: crucial factors for self-renewal, proliferation, and cell fate decisions. *J. Cell. Biochem.* **109**, 844–849 (2010).
- Angers, S. & Moon, R. T. Proximal events in Wnt signal transduction. *Nature Rev. Mol. Cell Biol.* **10**, 468–477 (2009).
- Takada, S. *et al.* Wnt-3a regulates somite and tailbud formation in the mouse embryo. *Genes Dev.* **8**, 174–189 (1994).
- Goessling, W. *et al.* Genetic interaction of PGE2 and Wnt signaling regulates developmental specification of stem cells and regeneration. *Cell* **136**, 1136–1147 (2009).
- McWhirter, J. R. *et al.* Oncogenic homeodomain transcription factor E2A-Pbx1 activates a novel WNT gene in pre-B acute lymphoblastoid leukemia. *Proc. Natl Acad. Sci. USA* **96**, 11464–11469 (1999).
- Bertrand, J. Y. *et al.* Haematopoietic stem cells derive directly from aortic endothelium during development. *Nature* **464**, 108–111 (2010).

8. Kissa, K. & Herbomel, P. Blood stem cells emerge from aortic endothelium by a novel type of cell transition. *Nature* **464**, 112–115 (2010).
9. Boisset, J. C. *et al.* *In vivo* imaging of haematopoietic cells emerging from the mouse aortic endothelium. *Nature* **464**, 116–120 (2010).
10. Bertrand, J. Y. *et al.* Definitive hematopoiesis initiates through a committed erythromyeloid precursor in the zebrafish embryo. *Development* **134**, 4147–4156 (2007).
11. Kissa, K. *et al.* Live imaging of emerging hematopoietic stem cells and early thymus colonization. *Blood* **111**, 1147–1156 (2008).
12. Lin, H. F. *et al.* Analysis of thrombocyte development in CD41-GFP transgenic zebrafish. *Blood* **106**, 3803–3810 (2005).
13. Yokota, T. *et al.* Tracing the first waves of lymphopoiesis in mice. *Development* **133**, 2041–2051 (2006).
14. Clements, W. K., Ong, K. G. & Traver, D. Zebrafish *wnt3* is expressed in developing neural tissue. *Dev. Dyn.* **238**, 1788–1795 (2009).
15. Nygren, M. K. *et al.* β -catenin is involved in N-cadherin-dependent adhesion, but not in canonical Wnt signaling in E2A-PBX1-positive B acute lymphoblastic leukemia cells. *Exp. Hematol.* **37**, 225–233 (2009).
16. Teh, M. T. *et al.* Role for WNT16B in human epidermal keratinocyte proliferation and differentiation. *J. Cell Sci.* **120**, 330–339 (2007).
17. Cirone, P. *et al.* A role for planar cell polarity signaling in angiogenesis. *Angiogenesis* **11**, 347–360 (2008).
18. Julich, D. *et al.* *beamter/deltaC* and the role of Notch ligands in the zebrafish somite segmentation, hindbrain neurogenesis and hypochord differentiation. *Dev. Biol.* **286**, 391–404 (2005).
19. Holley, S. A., Julich, D., Rauch, G. J., Geisler, R. & Nusselein-Volhard, C. *her1* and the *notch* pathway function within the oscillator mechanism that regulates zebrafish somitogenesis. *Development* **129**, 1175–1183 (2002).
20. Burns, C. E., Traver, D., Mayhall, E., Shepard, J. L. & Zon, L. I. Hematopoietic stem cell fate is established by the Notch-Runx pathway. *Genes Dev.* **19**, 2331–2342 (2005).
21. Hadland, B. K. *et al.* A requirement for Notch1 distinguishes 2 phases of definitive hematopoiesis during development. *Blood* **104**, 3097–3105 (2004).
22. Kumano, K. *et al.* Notch1 but not Notch2 is essential for generating hematopoietic stem cells from endothelial cells. *Immunity* **18**, 699–711 (2003).
23. Robert-Moreno, A., Espinosa, L., de la Pompa, J. L. & Bigas, A. RBPjk-dependent Notch function regulates *Gata2* and is essential for the formation of intra-embryonic hematopoietic cells. *Development* **132**, 1117–1126 (2005).
24. Robert-Moreno, A. *et al.* Impaired embryonic haematopoiesis yet normal arterial development in the absence of the Notch ligand Jagged1. *EMBO J.* **27**, 1886–1895 (2008).
25. Scheer, N. & Campos-Ortega, J. A. Use of the Gal4-UAS technique for targeted gene expression in the zebrafish. *Mech. Dev.* **80**, 153–158 (1999).
26. Scheer, N., Groth, A., Hans, S. & Campos-Ortega, J. A. An instructive function for Notch in promoting gliogenesis in the zebrafish retina. *Development* **128**, 1099–1107 (2001).
27. Ren, X., Gomez, G. A., Zhang, B. & Lin, S. *Scf* isoforms act downstream of *etsrp* to specify angioblasts and definitive hematopoietic stem cells. *Blood* **115**, 5338–5346 (2010).
28. Kemp, C., Willems, E., Abdo, S., Lambiv, L. & Leyns, L. Expression of all Wnt genes and their secreted antagonists during mouse blastocyst and postimplantation development. *Dev. Dyn.* **233**, 1064–1075 (2005).
29. Corrigan, P. M., Dobbin, E., Freeburn, R. W. & Wheadon, H. Patterns of Wnt/Fzd/LRP gene expression during embryonic hematopoiesis. *Stem Cells Dev.* **18**, 759–772 (2009).

Supplementary Information is linked to the online version of the paper at www.nature.com/nature.

Acknowledgements The authors wish to thank L. Zon, K. Poss, D. Kimelman, M. Lardelli, B. Appel, C. Burns, J. Campos-Ortega, D. Ransom, N. Trede, J. Lewis, M. Pack, S. Holley, C. Moens, B. Paw, R. Karlström and J. Waxman for probe constructs. L. Zon, R. Dorsky, S. Lin and S. Holley provided transgenic and mutant zebrafish lines. C. Weaver, K. Willert, K. J. P. Griffin, J. Bertrand, D. Stachura and Y. Lee provided critical evaluation of the manuscript. This research was funded by an AHA Postdoctoral Fellowship 0725086Y to W.K.C., an AHA Predoctoral Founders Affiliate Fellowship 0815732D to J.C.M., NIH R01-HL093467 to N.L. and NIH R01-DK074482, CIRM New Investigator Award, and March of Dimes 6-FY09-508 to D.T.

Author Contributions W.K.C. and D.T. designed all experiments. Whole-mount immunofluorescence, double fluorescence *in situ*, and Kaede-based fate mapping was performed by A.D.K. K.G.O. cloned and subcloned multiple constructs. J.C.M. and N.L. generated Notch reporter lines. All other experiments were performed by W.K.C. The manuscript was written by W.K.C. and edited by N.L. and D.T., with critical input as described in the Acknowledgments.

Author Information Reprints and permissions information is available at www.nature.com/reprints. The authors declare no competing financial interests. Readers are welcome to comment on the online version of this article at www.nature.com/nature. Correspondence and requests for materials should be addressed to D.T. (dtraver@ucsd.edu).

METHODS

Zebrafish husbandry, microinjections and heat shock. Zebrafish strains AB*, *Tg(TOP:GFP)^{w25}*, *Tg(-6.0itga2b:eGFP)^{la2}*, *Tg(hsp70l:Gal4)^{1.5kca4}*, *Tg(UAS:myc-Notch1a-intra)^{kca3}*, *Tg(tp1-MmHbb:EGFP)^{um14}*, *Tg(tp1-MmHbb:Kaede)^{um15}*, *Tg(cmyb:EGFP)^{ef169}*, *Tg(kdrl:RFP)^{la4}* and *dlc^{t1446/t1446}* (S. Holley) were maintained, crossed, injected, raised and staged as described³⁰, and in accordance with IACUC guidelines. The new line *Tg(tp1-MmHbb:Kaede)^{um15}* was generated by Tol2-mediated transgenic insertion of a transgene containing a previously described Notch-responsive promoter³¹ driving *Kaede* expression. Heat shocks were performed at the times indicated for 45 min at 37 °C, as previously described²⁰.

Cloning, constructs and probes. Both zebrafish *wnt16* isoforms (*wnt16-001* and *wnt16-002*, Zebrafish Information Network (ZFIN)) were amplified from AB* embryo cDNA at tailbud, 9-somite and 24 h.p.f., using primers (5' UTR-*wnt16-F* CAGGTGCTACATATTAGTCAGTGG, *wnt16-var.-F* GACATGG ATAATACCGGTTGTGGG, and *zWnt16-R* TTACTTGCAGGTGTCATGT CATTG) designed based on GenBank sequences NM_207096 and CD751181.1 and cloned to pCRII-TOPO-TA (Invitrogen) according to the manufacturer's instructions. Sequenced clones conform to subsequently deposited GenBank sequences NM_001100046.1 (*wnt16-001*) and BC066432.1 (*wnt16-002*), with no non-silent alterations. The *wnt16-001* form was re-cloned using the primers *gcatccGACATGGATAATACCGGTTGTG* and *ctcgagTACTTGCAGGTGTG CATGTC* to introduce 5' BamHI and 3' XhoI sites (PCR-added cut sites presented as lowercase in all primer sequences). *wnt16-001* and *wnt16-002* sequences were subcloned to pCS2+ (ref. 32) via BamHI/XhoI or EcoRI, respectively. Full-length *dlc* was amplified from 16-ss AB* cDNA using the primers *dlc-F* (ctcgagAA GATGGCTCGTGTTTTATTAAC) and *dlc-R* (tctagaCTATACCTCAGTAGC AAACACACG), TOPO-TA cloned, confirmed by sequencing, and subcloned to pCS2+. pCS2+ *wnt3*, pCS2+ *dnfgr1-eGFP* (K. Poss) and pBS *chd* (D. Kimelman) were described previously¹⁴. The following probe and expression constructs were gifts as indicated: pCS2+ *runx1* (C. Burns), pBK-CMV *scl* (L. Zon), pBK-CMV *cmyb* (L. Zon), pBS *kdrl* (D. Ransom), pBS *gata1* (D. Ransom), pCS2+ *gata2* (B. Paw), pCRII *rag1* (N. Trede), pBS *dlc* (J. Lewis), pBS *dld* (B. Appel), pCS2+ *dld* (S. Holley), pBS *jag1b* (M. Pack), pBS *jag2* (M. Pack), pCR-Script *notch1a* (J. Campos-Ortega), pCR-Script *notch1b* (M. Lardelli), pCR-Script *notch2* (B. Appel), pCR-Script *notch3* (M. Lardelli), pSPORT1 *etsrp* (S. Sumanas), pBS *nkx2.2* (R. Karlström), pCRII *gli1* (R. Karlström), pBS *ptc2* (R. Karlström), pBS *ptc1* (J. Waxman), pBS *prdm1a* (J. Waxman). The following probe constructs were amplified *de novo* and cloned to pCRII-TOPO-TA (Invitrogen) using primers as indicated: pCRII *myod* (*myod-F* AAGATGGAGTTGTGGGATATCC, *myod-R* AGAATTTAAAGCACTTGATAAATGG), pCRII *cdh5-frag* (*cdh5-probe-F* TGCCCTCCGACAAGGATGAAA, *cdh5-probe-R* ACCGAGGTCCCACTCAT GT), pCRII *cdh17/cb903* (*cb903/cdh17-F* GCGGATGATACAGGAACAGG, *cb903/cdh17-R* CTGAAGGCAGATGAAGCC), pCRII *col2a1a-frag* (*col2a1a-probe-F* CCACCTGGATTGACTGGACC, *col2a1a-probe-R* GTAGTGCTTGCA TGTTCCGTC), pCRII *vegfaa₁₆₅* (*vegfaa-long-F* GTTAATTTAGCGGATTCCG ACG, *vegfaa-short-R* GATCATCATCTGGCTTTTCAC), pCRII *shha* (*Bamshha-F* gcatccAAAATGCGGCTTTTGAC, *shha-R1-R* gaattcTCAGCTTGAGTT TACTGACATCC; subsequently subcloned to pCS2+), pCRII *foxc1a* (*foxc1a-F* GTCATGCAGGCGCTATT, *foxc1a-R* ctcgagTCAAAATTTGCTGCAGTCA TACAC), pCRII *foxc1b* (*foxc1b-F* gcatccACGATGCAGGCGGCTACCC, *foxc1b-R* TCAGAAGCTTGCTGCAGTCTATAC), pCRII *twist1b* (*twist1b-F* GAGATGCCGAAGAGCCCGCGC, *twist1b-R* ctcgagCTAGTGAGATGCAGA CATGGACC), pCRII *twist2* (*twist2-F* GAAATGGAAGAGAGTTCTAGCTC, *twist2-R* ctcgagCTAGTGGGACGACATCG). A *pax1* fragment corresponding exactly to the 1,080-bp open reading frame found in NM_001080592, which has been annotated as the zebrafish *Pax1* orthologue at NCBI Homologene (HomoloGene:4514), was amplified (R1-*pax1-F* gaattcAAAATGCTTTCGTGT TTTGCAGAG, *pax1-Xba-R* tctagaTTACGAGGATGAGGTAGAAAGGC) from 24 h.p.f. AB* cDNA to generate pCRII *pax1*. The *pax1* gene is located on chromosome 17 and shows syntenic conservation of the 5' neighbour (*Nkx2.2* in mouse and *NKX2.2* in human). The encoded protein is 69% identical and 90% similar to mouse and human PAX1. A 5' XhoI/ClaI fragment of pBS *efnb2a* (gift of C. Moens) was re-cloned to pBS to generate pBS *efnb2a-probe*. Digoxigenin- and fluorescein-labelled probes were generated as described previously³³ using 5' cut sites and RNA polymerases as appropriate (details available on request). Embryos were mounted and photographed as described¹⁴.

mRNA, morpholinos and injections. 5'-G-capped mRNAs were synthesized from NotI- or Asp718-(pCS2+ dlc) linearized pCS2+ constructs as described previously¹⁴, using the mMessage mMaching kit (Ambion). The following morpholino antisense oligonucleotides were synthesized by Gene Tools, LLC and suspended as 25 mg ml⁻¹ stocks in DEPC ddH₂O and diluted to injection strengths: W16MO1 AGGTTAGTTCTGTCAACCCACCTGTC, W16MO2 GCGT GGAATACCTACATCCAACCTTC, W16CoMO2 ('CoMO' in the text) AcGTT AGTTgTGTCAgCCAgCTcTC, lowercase letters denote mismatched bases, dldMO2 AAACAGCTATCATTAGTCGTCATCCAT (ref. 19), W11MO GAAAGT TCCTGTATTCTGTCAATGTC (ref. 34). Injections were performed as described previously¹⁴, and 0.1% phenol red (Sigma Aldrich) was included as an indicator. W16MO1 and W16MO2 were injected individually at 5 ng and combinatorially at 2 ng W16MO1 plus 3 ng W16MO2. In all depicted cases, both morpholinos caused the representative phenotypes shown, thus embryos are labelled 'W16MO'. A total of 5 or 7 ng of dldMO and W11MO were injected. 50 pg of *dlc* and/or *dld* mRNA were injected for rescue experiments.

Genomic and phylogenetic analyses. Alignments, genomic analyses and phylogenetic comparisons were performed as described previously¹⁴ using the following sequences: *wnt16l* NP_001093516.1, *mWnt16* NP_444346.3, *hWNT16a* NP_057171.2, *hWNT16b* NP_476509.1 and *hWNT4* NP_110388.2 (as the outgroup). Sequencing analysis was performed with Sequencher software (GeneCodes Corp.).

PCR genotyping and RT-PCR. Fixed, WISH-processed individual embryos had DNA isolated in lysis buffer (10 mM Tris, pH 8.3, 50 mM KCl, 0.3% Tween-20, 0.3% NP-40), 98 °C, 10 min, held at 4 °C to allow addition of proteinase K to a final concentration of 1 mg ml⁻¹, 18 h at 55 °C, 15 min at 98 °C. Presence of the *UAS:NICD* transgene was assessed by PCR using the primers E1B-F CATCGCGTCTCAGCCTCAC and Notch-R CGGAATCGTTTATTGGTGT CG (*T_m* 55 °C, extension time 45 s, 35 cycles), with *ef-1 α* -F GTGCTG TGCTGTGTTGCTG, *ef-1 α* -R TGTATGCGTGACTTCCTTG as a positive control (*T_m* 56 °C, extension time 30 s, 25 cycles). For RT-PCR, RNA was isolated from groups of 30 whole embryos at the stages indicated, and cDNA prepared as described previously¹⁴. PCR on cDNA was amplified using the primers *ef-1 α* (as above), *wnt16-RT1-F* FACTAAAGAGACAGCGTTTCATCC, *wnt16-RT1-R* AACT CATCTTTGGTGATAGGC, *wnt16-RT3-F* TTGTGGGATACATGCAGTCA and *wnt16-RT3-R* CACAGCTCCTTCTGCTTGTG with Taq polymerase (Invitrogen) at a *T_m* of 56 °C, extension times of 30 s, 38 cycles. Gels were imaged as described previously¹⁴.

Whole-mount *in situ* and antibody staining. Single and double enzymatic WISH was performed as described previously³³. Double fluorescence *in situ* were performed according to published protocols¹⁸. Whole-mount immunofluorescence was performed as described³⁵, using anti-Myc monoclonal 9E10 antibodies at 1:200 (Covance) and Dylight488 AffiniPure donkey anti-mouse IgG secondary antibodies (Jackson ImmunoResearch Laboratories) at 1:100.

Confocal, fluorescence microscopy, photoconversion and time-lapse imaging. Confocal images were acquired, essentially as described⁷. Photoconversion of *Kaede* proteins was performed using the Leica SP5 ROI and bleach functions on whole embryos, excluding heads, using a 405-nm laser line for 2 min. *Kaede* fluorescence was visualized using 488-nm and 543-nm laser lines. Fluorescence images of transgenic animals were acquired on a Leica DMI 6000 (Leica Microsystems) and time-lapse images were analysed and processed using Velocity software (Perkin-Elmer) as described previously³⁶.

- Westerfield, M. *The Zebrafish Book. A Guide for the Laboratory Use of Zebrafish* (Danio Rerio) (Univ. Oregon Press, 2004).
- Parsons, M. J. et al. Notch-responsive cells initiate the secondary transition in larval zebrafish pancreas. *Mech. Dev.* **126**, 898–912 (2009).
- Turner, D. L. & Weintraub, H. Expression of achaete-scute homolog 3 in *Xenopus* embryos converts ectodermal cells to a neural fate. *Genes Dev.* **8**, 1434–1447 (1994).
- Clements, W. K. & Kimelman, D. LZIC regulates neuronal survival during zebrafish development. *Dev. Biol.* **283**, 322–334 (2005).
- Lele, Z., Bakkers, J. & Hammerschmidt, M. Morpholino phenocopies of the *swirl*, *snailhouse*, *somitabun*, *minifin*, *silberblick*, and *pipetail* mutations. *Genesis* **30**, 190–194 (2001).
- Nüsslein-Volhard, C. & Dahm, R. *Zebrafish* (Oxford Univ. Press, 2002).
- Bertrand, J. Y., Kim, A. D., Teng, S. & Traver, D. CD41⁺ *cmyb*⁺ precursors colonize the zebrafish pronephros by a novel migration route to initiate adult hematopoiesis. *Development* **135**, 1853–1862 (2008).